KHz-rate volumetric voltage imaging of the whole Zebrafish heart

Leonardo Sacconi,[1,2,*] Ludovico Silvestri,[1,3] Esteban C. Rodríguez,[4] Gary A. B. Armstrong,[4] Francesco S. Pavone,[1,3] Alvin Shrier,[5] and Gil Bub[5,*]

[1]European Laboratory for Non-linear Spectroscopy, and National Institute of Optics, National Research Council, Sesto Fiorentino, Italy; [2]Institute for Experimental Cardiovascular Medicine, University Heart Center and Medical Faculty, University of Freiburg, Freiburg, Germany; [3]Department of Physics and Astronomy, University of Florence, Florence, Italy; [4]Department of Neurology and Neurosurgery, McGill University, Montreal, Canada; and [5]Department of Physiology, McGill University, Montreal, Canada

ABSTRACT   Fast volumetric imaging is essential for understanding the function of excitable tissues such as those found in the brain and heart. Measuring cardiac voltage transients in tissue volumes is challenging, especially at the high spatial and temporal resolutions needed to give insight to cardiac function. We introduce a new imaging modality based on simultaneous illumination of multiple planes in the tissue and parallel detection with multiple cameras, avoiding compromises inherent in any scanning approach. The system enables imaging of voltage transients *in situ*, allowing us, for the first time to our knowledge, to map voltage activity in the whole heart volume at KHz rates. The high spatiotemporal resolution of our method enabled the observation of novel dynamics of electrical propagation through the zebrafish atrioventricular canal.

WHY IT MATTERS   Cell voltage is an important biophysical parameter that is challenging to measure in 3D organs such as the heart. Simultaneous parallel excitation and emission detection microscopy is a new technique that illuminates tissue with several parallel light sheets and captures data using multiple cameras. We loaded intact zebrafish hearts with a voltage sensitive dye, allowing us to image voltage waves passing through seven planes in the tissue at very high speeds. Our 3D imaging studies revealed that under certain circumstances, electric impulses can backpropagate through specialized anatomical pathways that link the heart's chambers to re-excite the atria.

INTRODUCTION

Organs with excitable cells such as the heart and brain propagate voltage signals at high speed through spatially complex structures in three dimensions. Imaging activity in tissue volumes pose challenges that have been partially met in neural tissues by leveraging either the relative sparsity of active cells (1,2) or relying on measuring slowly varying ions such as calcium (3). These strategies are less viable in the heart, where cardiac function sensitively depends on waves of electrical activity rapidly propagating through dense layers of connected cardiac cells. Researchers have made headway measuring these waves using techniques that estimate activity in deep tissue using tomographic reconstruction (4,5) or that measure mechanical

contraction as a surrogate for voltage using ultrasound (6). In addition, light field microscopy, which images 3D spatial information of the incident light field in one sensor, is an emerging method for capturing volumetric data, but so far this technique has not captured voltage waves in intact tissue (7–9). The most promising approach for directly measuring voltage at cellular scales in tissue volumes is light-sheet microscopy (LSM), as it can capture confocal sections with the long integration times needed to measure activity from voltage-sensitive dyes. LSM-based volumetric imaging strategies either rely on rapidly scanning the sheet through the sample (10–15), use gating or correlation methods to capture information at different points in the cardiac cycle over many successive contractions (16–19), or use parallel illumination planes to increase acquisition rates (20,21). However, these approaches have fundamental limitations. Fast scanning methods trade integration time for high acquisition speed (11,14), and correlation methods can only image regularly repeating events (16). These methods
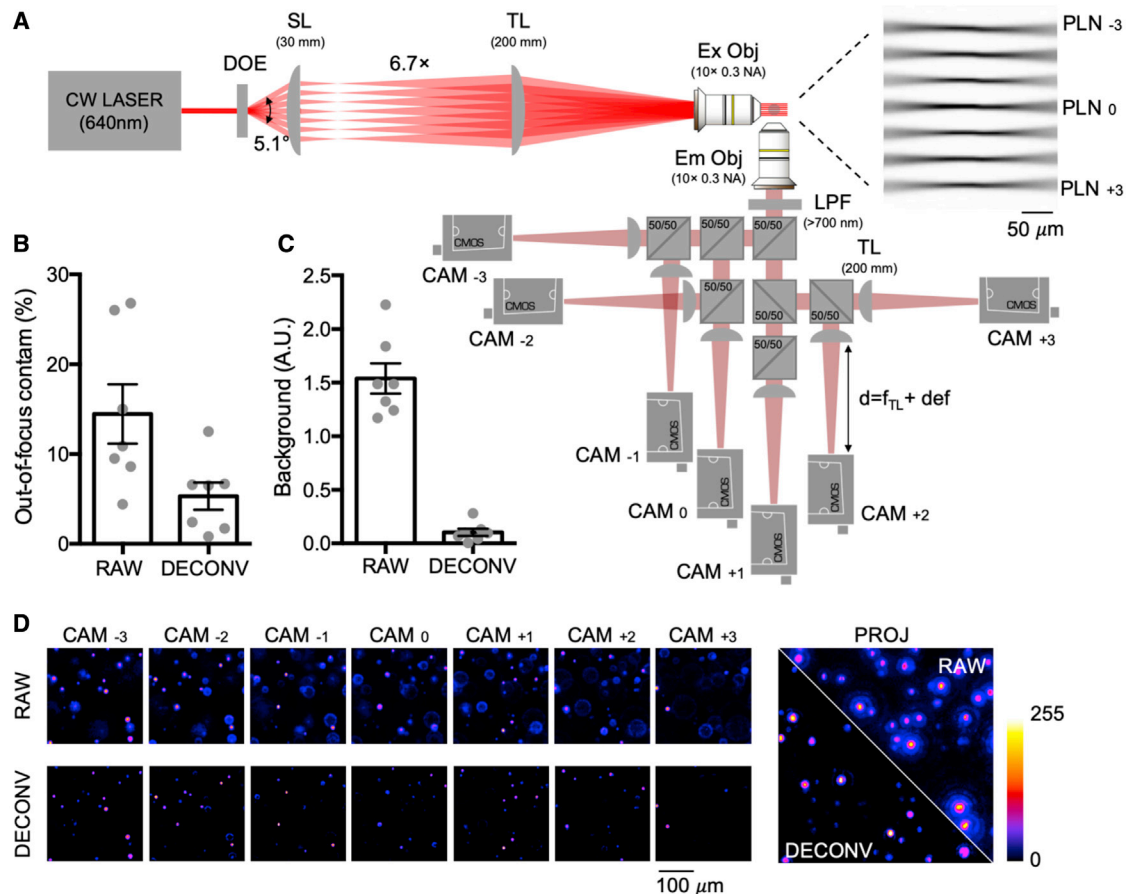
FIGURE 1 SPEED microscopy. (A) Optical scheme: a 640-nm continuous wave (CW) laser beam is split and shaped as a light sheet spaced 43 μm apart by diffractive optical element (DOE) and coupled by scan lens (SL) and tube lens (TL) to a 10× objective; the inset shows the real excitation light sheets imaged from an axis orthogonal to both excitation and detection, using a fluorescent gel; an orthogonally placed objective collects emitted fluorescence, which is then split by a cascade of 50:50 unpolarized beam splitters and focused by detection tube lenses (TL) onto cameras placed at different focal positions (f_{TL} + variable defocus); a long-pass filter (LPF) placed just after the detection objective blocks excitation light. A picture of the assembled system is shown in Fig. S2. (B) Quantification of out-of-focus light contamination to images (raw versus deconvoluted): off-focus contamination was quantified using the reverse ratio between the fluorescence signal collected by the camera associated with the light-sheet that excites a fluorescence bead and the fluorescence signal collected by the proximal out-of-focus plane. (C) Quantification of background light intensity (raw versus deconvoluted): The background was quantified after normalization of the maximum intensity signal between the raw and deconvolved images. (D) Images of fluorescent beads from the seven cameras (raw versus deconvoluted) with a zoomed view of a maximum-intensity projection. Error bars are ± SEM. Measurements of bead diameter in each plane are given in Fig. S4.

would find detection of irregular, sparse cardiac events, such as early after-depolarizations (EADs) challenging. EADs occur in myocytes due to imbalances in cardiac action potential repolarization kinetics, which may trigger a macroscopic propagating wave: EADs are associated with potentially fatal arrhythmias and are thus active areas of research (22). Finally, current parallel plane strategies either greatly restrict the number and location (21) of imaging planes, or when multiplexing data from several planes onto a single detector (20), they must increase acquisition time proportionately to the number of planes to maintain signal quality. Although some parallel plane architectures could, in principle (23,24), operate at high rates using specialized high-speed cameras, so far there has been no demonstration of volumetric data capture with the

signal quality needed to track voltage transients at physiologically relevant timescales.

Simultaneous parallel excitation and emission detection (SPEED) microscopy is a new technique that captures data from multiple light sheets on multiple sensors in real time. Conventional LSM achieves optical sectioning by ensuring that all fluorescence originates from a single plane. In our system, multiple parallel light sheets are projected into the sample and each plane is imaged by its own camera (Fig. 1 A). Each camera captures in-focus light originating from a single light sheet along with out-of-focus light from adjacent ones. Standard deconvolution algorithms are used to redirect out-of-focus signal to the correct plane to improve optical sectioning. There are two key benefits of this configuration over other parallel-

plane approaches. First, we can have many illumination planes that fully cover the imaging volume, allowing capture of z-stacks without scanning. Second, the use of multiple detectors allows for high acquisition rates without a specialized high-speed sensor. In addition, the multisensor architecture allows visualization of data in real time during experimental runs while avoiding trade-offs in signal quality, spatial resolution, and dynamic range that are often associated with encoding data from multiple sources on one camera (21).

The zebrafish is emerging as a popular experimental model for cardiac research, in part because the heart has voltage transients that are similar to those in humans and its small size makes the entire heart accessible to volumetric tissue imaging techniques that allow *in situ* imaging of embedded structures. Voltage transients on the heart's surface (25,26) or in single planes (27) within the tissue have been imaged at high spatial and temporal resolutions. Current volumetric tissue imaging modalities are, however, too slow to capture electrical activity at millisecond resolution with sufficient spatial detail to image propagation in the zebrafish heart.

MATERIALS AND METHODS

Zebrafish

Wild-type AB zebrafish (*Danio rerio*) were bred and maintained according to standard procedures (28). This study was performed in accordance with the guidelines of the Canadian Council for Animal Care and conducted at the Montreal Neurological Institute at McGill University in Montreal, Quebec, Canada. All experiments were approved by the Montreal Neurological Institute-Hospital Animal Care committee, and Dr. Gary Armstrong currently holds an approved Animal Use Protocol #2017-7890. Experiments were performed on sexually undifferentiated zebrafish larvae aged 2 weeks postfertilization. Zebrafish were anesthetized with tricaine methanesulfonate at a concentration of 250 mg/L, decapitated, and the hearts extracted using fine forceps. Hearts were kept at room temperature in standard fish system water with 10 mM glucose before imaging.

Dye loading and imaging

Excised hearts were placed in 1 μM Di-4-ANBDQPQ (29) (Potentiometric Probes, USA) in Evans for 5 min and were placed in a dish containing 2% solution low melting point agarose (Sigma) dissolved in Evans solution. As the gel started to set, the heart was positioned into a glass capillary tube (Red Tip Brand, 1 mm inner diameter, Sherwood Medical Industries cat:21,112, and Fig. S6). An ~1-mm segment of agar containing the heart was pushed out and suspended from the capillary tube in a square-walled plastic cuvette (BrandTech, 1.5 mL capacity, cat:759150) containing 1 mL Evans for recording. For most experiments, 5 μM blebbistatin (Tocris Biosciences) was added to the agarose and recording solution to arrest contraction. For the experiments presented in Fig. 3, potassium channel blocker E4031 (Tocris Biosciences, final concentration 20 μM), cholinergic agonist carbachol (final concentration 1 μM), and β-adrenoreceptor agonist isoproterenol (Tocris Biosciences, final concentration 1 μM) were added directly to the cuvette from diluted stock solutions. Isoproterenol induced afterdepolarizations by activating the cardiac

beta receptor, leading to an increase in cAMP via upregulation of adenylyl cyclase activity (30,31). Isoproterenol's role was confirmed by blocking its effect using carbachol, which activates muscarinic receptors resulting in downregulation of adenylyl cyclase.

Software: hardware control

The seven cameras were controlled using a custom software interface (available at https://doi.org/10.5281/zenodo.5800192) written in Java and Basler's free Pylon SDK. The software allows simultaneous viewing of the seven cameras for focusing and acquisition. Alignment was achieved by writing a wrapper around Fiji plugin (Register_Virtual_Stack_MT.java; https://imagej.net/Register_Virtual_Stack_Slices) to find pixel offsets for each camera after focusing on a high-contrast image target, which were then used to select a region from each camera for recording. This enabled us to have pixel-accurate alignment without the added complexity of a dedicated two-axis stage for each camera. The number of pixels in the recording region sets bounds on the frame rate due to data transfer limitations in the USB cameras used in this study: we used a 400 x 400 pixel region for 500-Hz imaging and a 128 x 128 pixel region to image at 1000 Hz (see Fig. S7), where the location of this region on each sensor is determined by the alignment step. During image acquisition, cameras were synchronized to a timing pulse set using an Arduino Uno microcontroller, which also triggered LED and laser illumination. A set of 1000 frames from each camera was saved in a circular buffer and transferred to disk as a single file for each record.

Analysis

Data was deconvolved by first converting image data to tiffs and processing using commercial software (Huygens Professional version 19.04, Scientific Volume Imaging). We used blind Richardson-Lucy deconvolution with maximum 40 iterations, assuming the same PSF for all the planes. Initial estimate of the PSF was computed from the illumination and detection numerical apertures (NAs), resulting in an Airy pattern in the plane and a Gaussian profile along the detection axis. As these deconvolution algorithms may add artifacts, we confirmed that action potential timing can be reliably reconstructed by using a simulated data set (Fig. S5). 3D meshes (Fig. 3 *B*) were generated by first capturing a high-resolution (1.25 μm per plane) scan using a single light sheet (see supporting material: High Resolution Scanning), and then generating a 3D mesh from this data using Fiji's 3D viewer plugin (v 4.02, https://imagej.net/3D_Viewer (32)). This mesh was then exported into custom written software that extended Processing's (https://www.processing.org) PApplet class and its P3D openGL environment to display the mesh and overlay activation waves captured from the seven planes. Isochronal maps (Figs. 2 *F*, *G*, and 3 *G*, as well as S7C and S8), which show wave location at different time points, were generated by first spatially binning data to give 200 x 200 pixel images for each view, normalizing data so that temporal transients for each pixel have the same magnitude, filtering the data with a running five-frame temporal and five-pixel-radius spatial median filters before using a marching squares algorithm to locate wavefronts based on the threshold-crossing time for each pixel. For Figs. 3 *G* and S8, backpropagation was measured by averaging the signals from two cameras and averaging signals from three successive EADs before generating the isochronal maps.

RESULTS

We demonstrate SPEED using seven light sheets statically generated from a 645-nm laser light (OxxiusLBX-638-180-CSB-PPA) by a diffractive optical element
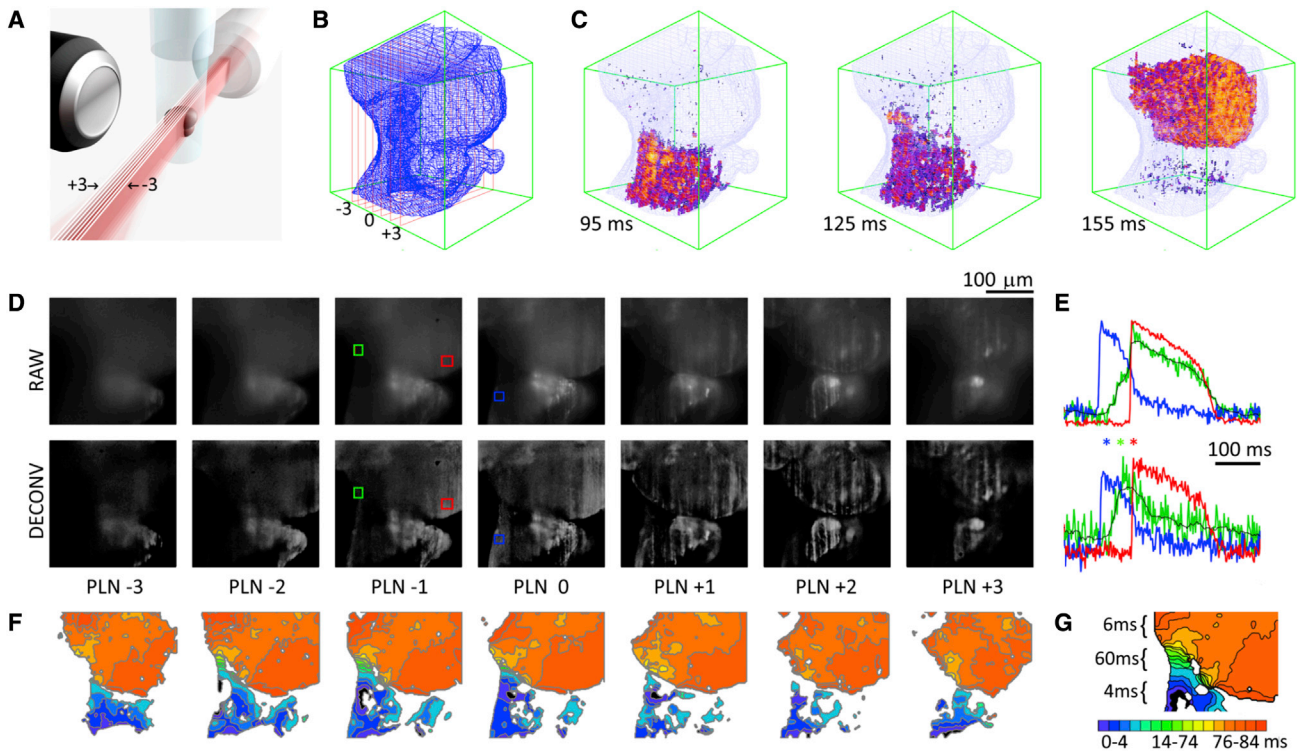
Figure360▷ FIGURE 2   For a Figure360 author presentation of this figure, see https://doi.org/10.1016/j.bpr.2022.100046.
(A) Orientation of sample relative to the seven light sheets; (B) Surface mesh generated from high resolution z-stack; (C) Propagation of voltage transients in the seven planes at 95 ms, 125 ms, and 155 ms; (D) Comparison of the seven planes (PLN-3 through PLN+3) for raw and deconvoluted data sets; with ROIs (red green and blue colored boxes) in PLN -1 and 0; (E) Action potential morphology from atrium (blue), ventricle (red), and AV canal region (green) for raw and deconvolved datasets from the ROIs in (D). Blue, green, and red asterisks symbols correspond to 95 ms, 125 ms, and 155 ms to show the relative timing in the maps shown in (C); (F) Isochronal maps show propagation through atrial, AV, and ventricular tissues; (G) A close up view showing a map of the slow conduction through the AV region.

(HoloeyeDE-R 251) and projected onto a 250 × 250 × 250 μm volume by a 10× objective (Fig. 1 A). Fluorescent images are collected by seven machine vision cameras (Basler acA720-520 μm) in parallel and processed using standard deconvolution algorithms (Huygens Professional). These algorithms transfer out-of-focus signal to the correct image plane to further increase contrast and optical sectioning. We demonstrate the effectiveness of this approach using a sample phantom containing fluorescent beads (Fig. 1 B−D).

We positioned explanted zebrafish hearts loaded with red-shifted voltage-sensitive dye (Di-4-ANBDQPQ,1 μM) into the SPEED microscope as shown in Fig. 2 A. Fluorescence was captured from seven 400 × 400 pixel planes (Fig. 2 A and D) simultaneously at over 500 frames/s, allowing us to map activity in a 250 μm^3 volume (Fig. 2 B and C). Action potentials from three regions of interests (ROI) are shown for the raw and deconvolved data sets in Fig. 2 E, with one ROI positioned over atrial tissue (blue), one over the ventricular tissue (red), and a third positioned in tissue between these (green) in a region that corresponds to the atrioventricular (AV) canal. Although action potential morphology for atrial (blue) and ventricular (red) ROIs is clearly

resolvable in the raw data set, the AV action potential shape is corrupted by signal from overlapping layers. Deconvolution reveals a voltage transient morphology in slowly conducting tissue that is distinct from that found in atrial or ventricular tissues. The deconvolved data set is then used to generate isochronal maps showing propagation in each plane. We note that deconvolution reduces the apparent signal quality (Fig. 2 E), which leads to a lack of smoothness of the isochronal maps. However the signal still has sufficient detail to map conduction through the slowly conducting AV canal (Fig. 2 F and G). Propagation in the entire imaged volume is then visualized in 3D by overlaying the seven planes on a conventionally acquired z-stack (Fig. 2 B, C, Movies S1A, and S1B).

SPEED's light efficiency allows long record times without apparent phototoxicity or bleaching, enabling data capture for over 90 min with little loss in signal quality. We leveraged the system's ability to capture long records to make an experimental model of an arrhythmia where waves backpropagate from the ventricles to the atria. Repolarization kinetics were pharmacologically altered in the zebrafish hearts resulting in prolonged ventricular action potentials (Fig. 3 D)
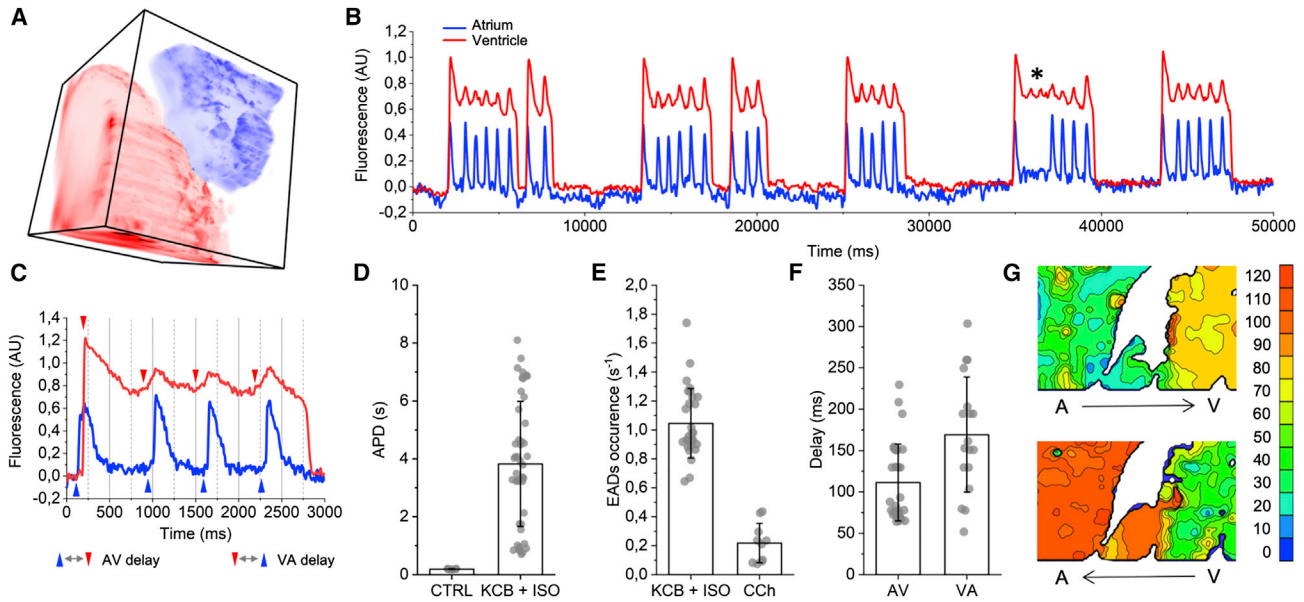
FIGURE 3 (*A*) Volume map of atrial (blue) and ventricular (red) regions obtained from a high-resolution $250 \times 250 \times 250\ \mu m$ z-stack (see supporting material: High Resolution Scanning). (*B*) Action potentials from ventricular and atrial regions (taken by averaging the entire atrial and ventricular regions from imaging plane P0) show backpropagation of ventricular early afterdepolarizations (EAD) activating atrial tissue (star: EADs without backpropagation). (*C*) Ventricular EAD onset (red arrows) occurs before atrial activations (blue arrows). (*D*) Effect of E4031 (KCB) and isoproterenol (ISO) on action potential duration in the ventricle. (*E*) EADs per action potential over all records in E4031 and isoproterenol treated hearts: EAD frequency greatly reduced by carbachol (CCh). (*F*) Delay between atrium and ventricle is slightly lower than the backpropagation delay between the ventricle and atrium. (*G*) Isochronal maps of a $170 \times 100\ \mu m$ cardiac section with isochrones drawn every 10 ms show atrial (A) to ventricular (V) propagation direction for the first atrial beat in Fig C (top) and backpropagation from the ventricle to the atria for subsequent EAD triggered beats (bottom). Error bars are $\pm$ SD. See Fig. S8 for the entire $250 \times 250\ \mu m$ field of view.

and EADs (Fig. 3 *E*). EADs generate extrasystolic waves that backpropagate through the AV canal and re-excite the atrium (Figs. 3 *B*, *C*, *G*, and S8). Conduction times between the ventricle and atrium are consistent but slightly longer (Fig. 3 *F* and *G*) than those measured between the atria and ventricles during normal rhythms, suggesting that the AV canal is optimized for propagating waves in one direction or that the AV tissue is only partially repolarized. Interestingly, increased ventricular to atrial conduction times are also observed in human hearts (33). Further study is needed to determine whether the mechanisms for direction dependent conduction times in these systems are the same.

DISCUSSION

SPEED's low phototoxicity and high signal quality is a consequence of having an architecture that maximizes sensor integration times using true parallel volumetric acquisition. Light-sheet imaging has advantages in capturing dynamic events from weakly fluorescent tissue as exposure times for each pixel can be far longer than a scanning system at a similar resolution (34). SPEED's architecture extends light-sheet's simultaneous imaging paradigm from 2D to 3D, allowing cap-

ture of z-stacks in thick samples in the time frame of a single camera exposure. The use of multiple cameras removes frame-rate bottlenecks associated with using a single large sensor while allowing visualization of optical sections during acquisition, which can be improved offline with deconvolution.

The system was designed to image a $250 \times 250 \times 250\ \mu m$ cube at high frame rates to capture propagation in a zebrafish heart. We used low-cost high-speed cameras that enabled us to access the entire sensor (5×3.7 mm at VGA resolution) to select 400×400 pixel regions that were aligned to image the same field of view at 0.5 KHz. We used a 10x objective ("Em Obj" in Fig. 1) with an NA of 0.3 for a theoretical radial PSF of the order of $1.5\ \mu m$ sampled at $0.7\ \mu m$. The same model objective ("Ex Obj" in Fig. 1) was used to generate multiple light sheets. In this pilot study, we opted to use seven planes generated by a low-cost plastic-based diffractive optical element (DOE). The DOE produces an angular deviation between each plane of the order of 0.85° and, after an angular demagnification of 6.7x, generates seven equally spaced illumination planes (of the order of 45 um between each plane) after the excitation objective lens. The NA of the excitation objective was halved by reducing the entrance pupil to generate light sheets with a depth

of focus compatible with the field of view of detection optics. The light sheets generated using this method are heterogeneous (see Fig. S3), which when coupled to the apparent reduction in signal quality imposed by deconvolution (Fig. 2 *E*), may ultimately pose limits on the resolution of the system. Despite these limitations, the SPEED microscope was able to resolve conduction in fine anatomical structures in the zebrafish heart.

We demonstrated our imaging system in zebrafish hearts as its popularity as a model system for studying cardiac dynamics is growing. Indeed, there are several studies that use voltage-sensitive dyes to map propagation in the zebrafish heart (35–38), but they all rely on measuring activity at the surface, and none are able to image interior structures such as the AV canal. SPEED can both capture fast dynamics of interior structures (Fig. 2) and perform longer-duration experiments (Fig. 3) in cardiac preparations. Although we have optimized SPEED for imaging zebrafish cardiac dynamics, it may be possible to adapt the microscope for high-speed volumetric imaging of other excitable tissues including the central nervous system. Such adaptations may include changing the way light sheets are generated: the quality of the light sheets produced by the DOI may adversely impact data collection in tissues with sparse fluorescent sources such as neural tissues. With suitable optimization (e.g., using Bessel beams (39) or an mSPIM (40) approach), SPEED could open the possibility to directly investigate electrical activity across neuronal populations, elucidating computational rules that remain hidden in the low temporal resolution of calcium indicators (41,42). Although in principle SPEED is not restricted to a specific illumination wavelength, our implementation with red light paves the way for effective coupling with optogenetic stimulation with blue light with negligible cross talk. The unique possibility of combining fast volumetric voltage imaging with the genetic specificity of channelrhodopsin opens research possibilities that are difficult to overestimate. For instance, spatiotemporal neuronal activation patterns related to a specific stimulus or experience could be reproduced using 3D holographic photostimulation (43) to investigate complex neuronal networks using a truly electrical pump-and-probe approach. A similar approach could be applied to cardiovascular research to disentangle the various roles that nonmyocyte cardiac cell populations (44–46) have in modulating cardiac wave dynamics in physiological and pathological conditions.

SUPPORTING MATERIAL

Supporting material can be found online at https://doi.org/10.1016/j.bpr.2022.100046.

AUTHOR CONTRIBUTIONS

L. Sacconi: original concept; G.B. and L. Sacconi: system construction and programming; G.A.B.A. and E.C.R.: cardiac sample preparation; G.B., L. Sacconi, and A.S.: designed and performed experiments; G.B., L. Sacconi, and L. Silvestri: data analysis; F.S.P. contributed new analytic tools; all authors contributed to writing the document and data interpretation.

DECLARATION OF INTERESTS

The authors declare no competing interests.

REFERENCES

1. Pnevmatikakis, E. A., D. Soudry, …, L. Paninski. 2016. Simultaneous denoising, deconvolution, and demixing of calcium imaging data. *Neuron.* 89:285.

2. Yang, W., J. E. Miller, …, D. S. Peterka. 2016. Simultaneous multiplane imaging of neural circuits. *Neuron.* 89:269.

3. Stosiek, C., O. Garaschuk, …, A. Konnerth. 2003. In vivo two-photon calcium imaging of neuronal networks. *Proc. Natl. Acad. Sci. U S A.* 100:7319–7324.

4. Khait, V. D., O. Bernus, …, A. M. Pertsov. 2006. Method for the three-dimensional localization of intramyocardial excitation centers using optical imaging. *J. Biomed. Opt.* 11:034007.

5. Hillman, E. M., O. Bernus, …, A. Pertsov. 2007. Depth-resolved optical imaging of transmural electrical propagation in perfused heart. *Opt. Express.* 15:17827.

6. Christoph, J., M. Chebbok, …, S. Luther. 2018. Electromechanical vortex filaments during cardiac fibrillation. *Nature.* 555:667–672.

7. Wagner, N., F. Beuttenmueller, …, A. Kreshuk. 2021. Deep learning-enhanced light-field imaging with continuous validation. *Nat. Methods.* 18:557–563.

8. Wagner, N., N. Norlin, …, R. Prevedel. 2019. Instantaneous isotropic volumetric imaging of fast biological processes. *Nat. Methods.* 16:497–500.

9. Wang, Z., L. Zhu, …, P. Fei. 2021. Real-time volumetric reconstruction of biological dynamics with light-field microscopy and deep learning. *Nat. Methods.* 18:551–556.

10. Dunsby, C. 2008. Optically sectioned imaging by oblique plane microscopy. *Opt. Express.* 16:20306–20316.

11. Voleti, V., K. B. Patel, …, E. M. C. Hillman. 2019. Real-time volumetric microscopy of in vivo dynamics and large-scale samples with SCAPE 2.0. *Nat. Methods.* 16:1054–1062.

12. Tomer, R., K. Khairy, …, P. J. Keller. 2012. Quantitative high-speed imaging of entire developing embryos with simultaneous multi-view light-sheet microscopy. *Nat. Methods.* 9:755–763.

13. Vladimirov, N., Y. Mu, ..., M. B. Ahrens. 2014. Light-sheet functional imaging in fictively behaving zebrafish. *Nat. Methods.* 11:883–884.

14. Chen, B. C., W. R. Legant, ..., E. Betzig. 2014. Lattice light-sheet microscopy: imaging molecules to embryos at high spatiotemporal resolution. *Science.* 346:1257998.

15. Ahrens, M. B., M. B. Orger, ..., P. J. Keller. 2013. Whole-brain functional imaging at cellular resolution using light-sheet microscopy. *Nat. Methods.* 10:413–420.

16. Taylor, J. M., C. J. Nelson, ..., M. A. Denvir. 2019. Adaptive prospective optical gating enables day-long 3D time-lapse imaging of the beating embryonic zebrafish heart. *Nat. Commun.* 10:1–15.

17. Lee, S., C. Vinegoni, ..., R. Weissleder. 2012. Real-time in vivo imaging of the beating mouse heart at microscopic resolution. *Nat. Commun.* 3:1054.

18. Mickoleit, M., B. Schmid, ..., J. Huisken. 2014. High-resolution reconstruction of the beating zebrafish heart. *Nat. Methods.* 11:919–922.

19. Weber, M., N. Scherf, ..., J. Huisken. 2017. Cell-accurate optical mapping across the entire developing heart. *Elife.* 6:e28307.

20. Ren, Y. X., J. Wu, ..., K. K. Tsia. 2020. Parallelized volumetric fluorescence microscopy with a reconfigurable coded incoherent light-sheet array. *Light Sci. Appl.* 9:1–11.

21. Dean, K. M., P. Roudot, ..., R. Fiolka. 2017. Imaging subcellular dynamics with fast and light-efficient volumetrically parallelized microscopy. *Optica.* 4:263.

22. Weiss, J. N., A. Garfinkel, ..., Z. Qu. 2010. Early afterdepolarizations and cardiac arrhythmias. *Heart Rhythm.* 7:1891–1899.

23. Ma, Q., B. Khademhosseinieh, ..., Z. Liu. 2016. Three-dimensional fluorescent microscopy via simultaneous illumination and detection at multiple planes. *Sci. Rep.* 6:1–8.

24. Xiao, S., H. Gritton, ..., J. Mertz. 2020. High-contrast multifocus microscopy with a single camera and z-splitter prism. *Optica.* 7:1477–1486.

25. van Opbergen, C. J. M., C. D. Koopman, ..., T. P. de Boer. 2018. Optogenetic sensors in the zebrafish heart: a novel in vivo electrophysiological tool to study cardiac arrhythmogenesis. *Theranostics.* 8:4750.

26. Stoyek, M. R., T. A. Quinn, ..., F. M. Smith. 2016. Zebrafish heart as a model to study the integrative autonomic control of pacemaker function. *Am. J. Physiol. Heart Circ. Physiol.* 311:H676–H688.

27. Hou, J. H., J. M. Kralj, ..., A. E. Cohen. 2014. Simultaneous mapping of membrane voltage and calcium in zebrafish heart in vivo reveals chamber-specific developmental transitions in ionic currents. *Front. Physiol.* 5:344.

28. Westerfield, M. 1995. The Zebrafish Book: A Guide for the Laboratory Use of Zebrafish (Brachydanio rerio). University of Oregon Press.

29. Matiukas, A., B. G. Mitrea, ..., L. M. Loew. 2007. Near-infrared voltage-sensitive fluorescent dyes optimized for optical mapping in blood-perfused myocardium. *Heart Rhythm.* 4:1441–1451.

30. Shimizu, W., T. Ohe, ..., K. Shimomura. 1991. Early afterdepolarizations induced by isoproterenol in patients with congenital long QT syndrome. *Circulation.* 84:1915–1923.

31. Zhao, Z., G. J. Babu, ..., L. H. Xie. 2015. Overexpression of adenylyl cyclase type 5 (AC5) confers a proarrhythmic substrate to the heart. *Am. J. Physiol. Heart Circ. Physiol.* 308:H240–H249.

32. Schmid, B., J. Schindelin, ..., M. Heisenberg. 2010. A high-level 3D visualization API for Java and ImageJ. *BMC Bioinformatics.* 11:274.

33. Goldreyer, B. N., and J. T. Bigger. 1970. Ventriculo-atrial conduction in man. *Circulation.* 41:935–946.

34. Hillman, E. M. C., V. Voleti, ..., H. Yu. 2019. Light-sheet microscopy in neuroscience. *Annu. Rev. Neurosci.* 42:295–313.

35. Lin, E., A. Ribeiro, ..., G. F. Tibbits. 2014. Optical mapping of the electrical activity of isolated adult zebrafish hearts: acute effects of temperature. *Am. J. Physiol. Regul. Integr. Comp. Physiol.* 306:R823–R836.

36. Stoyek, M. R., and T. A. Quinn. 2018. One fish, two fish, red fish, blue fish*: zebrafish as a model for cardiac research. *Prog. Biophys. Mol. Biol.* 138:1–2.

37. Stoyek, M. R., E. A. Rog-Zielinska, and T. A. Quinn. 2018. Age-associated changes in electrical function of the zebrafish heart. *Prog. Biophys. Mol. Biol.* 138:91–104.

38. Sedmera, D., M. Reckova, ..., R. P. Thompson. 2003. Functional and morphological evidence for a ventricular conduction system in zebrafish and Xenopus hearts. *Am. J. Physiol. Heart Circ. Physiol.* 284:H1152–H1160.

39. Müllenbroich, M. C., L. Turrini, ..., F. S. Pavone. 2018. Bessel beam illumination reduces random and systematic errors in quantitative functional studies using light-sheet microscopy. *Front. Cell. Neurosci.* 12:315.

40. Huisken, J., and D. Y. Stainier. 2007. Even fluorescence excitation by multidirectional selective plane illumination microscopy (mSPIM). *Opt. Lett.* 32:2608.

41. Quirin, S., N. Vladimirov, ..., M. B. Ahrens. 2016. Calcium imaging of neural circuits with extended depth-of-field light-sheet microscopy. *Opt. Lett.* https://doi.org/10.1364/OL.41.000855.

42. Peterka, D. S., H. Takahashi, and R. Yuste. 2011. Imaging voltage in neurons. *Neuron.* 69:9–21.

43. Hernandez, O., E. Papagiakoumou, ..., V. Emiliani. 2016. Three-dimensional spatiotemporal focusing of holographic patterns. *Nat. Commun.* 7:1–11.

44. Dutta, S., A. Mincholé, ..., B. Rodriguez. 2016. Early afterdepolarizations promote transmural reentry in ischemic human ventricles with reduced repolarization reserve. *Prog. Biophys. Mol. Biol.* https://doi.org/10.1016/j.pbiomolbio.2016.01.008.

45. Prando, V., F. Da Broi, ..., M. Mongillo. 2018. Dynamics of neuroeffector coupling at cardiac sympathetic synapses. *J. Physiol.* 596:2055–2075.

46. Hulsmans, M., S. Clauss, ..., M. Nahrendorf. 2017. Macrophages facilitate electrical conduction in the heart. *Cell.* 169:510–522.e20.